Front. Phys. China (2006) 2: 219–224
DOI 10.1007/s 11467-006-0002-3

RESEARCH ARTICLE

CAI Yang-jian, ZHU Shi-yao

Coincidence imaging and interference with coherent Gaussian beams

Abstract we present a theoretical study of coincidence imaging and interference with coherent Gaussian beams . The equations for the coincidence image formation and interference fringes are derived，from which it is clear that the imaging is due to the corresponding focusing in the two paths . The quality and visibility of the images and fringes can be high simultaneously . The nature of the coincidence imaging and interference between quantum entangled photon pairs and coherent Gaussian beams are different . The coincidence image with coherent Gaussian beams is due to intensity-intensity correspondence，a classical nature，while that with entangled photon pairs is due to the amplitude correlation a quantum nature.

Keywords coincidence imaging and interference, coherent Gaussian beam, optics

PACS numbers 42.25.Hz, 42.25.Kb, 42.30.-d, 42.50.-p

In coincidence imaging (or interference)，an object(or slits) in one path produces an image (or fringes) in the measurement of coincident counting rates，which was first experimentally observed in 1995 with entangled photon pairs [1–2]. In the coincidence imaging or interference with the quantum source(the quantum case)，which was called ghost imaging，the image formation depends on both paths . The coincidence imaging with a classical coherent source，a laser beam，(the classical case) was experimentally observed in 2002 [3], which induced discussions [4–12]. More recently，R.Bennink *et al*. experimentally observed both the coincidence imaging and interference with classical coherent sources[13]. In this paper，we are going to simulate the coincidence imaging and interference using coherent Gaussian beams . Effect of the beam widths on the quality of the image and interference fringes is illustrated in detail . Differences between the coincidence imaging and interference with classical light and entangled photon pairs are discussed in detail .

Selected from *Acta Sinica Quantum Optica*, 2005, 11(4)(in Chinese)

CAI Yang-jian(✉)，ZHU Shi-yao
Department of Physics，Hong Kong Baptist University，Hong Kong，China；Institute of Optics，Department of Physics，ZheJiang University，Hangzhou，310027，China
E-mail:cyj@zju.edu.cn

1 Coincidence imaging with coherent Gaussian beams

The scheme for the coincidence imaging with the coherent source is the same as in Ref .[13]shown in Fig. 1 . The

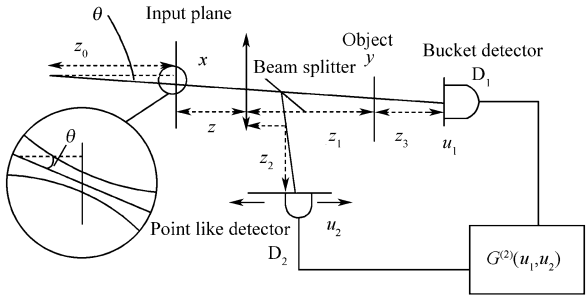

Fig .1 The scheme for coincidence imageing with coherent Gaussian beam

coherent source can be represented by a coherent Gaussian beam. The coherent Gaussian beam，which can be rotated，first passes through a lens with focal length f，and then is split by a beam splitter into two beams which propagate through two paths to two detectors (D_1 and D_2)，respectively . In path one(from the source plane x to D_1)，between the beam splitter and D_1 ，there is an object with transmision function $H(v)$，and D_1 is a bucket detecor . In path two(from the source plane x to D_2)，from the beam splitter to D_2 is a free space，and D_2 is a point-like detector which is mounted on a moving stage . The coincident counting rate is proportional to，the second order correlation function with integration over u_1 (because of the bucket detector)，

$G^{(2)}(u_2)=\int_{-\infty}^{+\infty}\mathrm{d}u_1 G^{(2)}(u_1,u_2)$. According to optical theory for the coherent Gaussian beams [14–15], we have

$$G^{(2)}(u_1,u_2)=\langle E(u_1)E(u_2)E^*(u_2)E^*(u_1)\rangle=\langle I(u_1)\rangle\langle I(u_2)\rangle$$
$$=\left|\int_{-\infty}^{\infty}E(x_1)h_1(x_1,u_1)\mathrm{d}x_1\right|^2\left|\int_{-\infty}^{\infty}E(x_2)h_2(x_2,u_2)\mathrm{d}x_2\right|^2 \quad (1)$$

where $h_1(x_1, u_1)$, $h_2(x_2, u_2)$ are the response functions of the two paths, respectively .

In the source plane(x), which is the waist plane of the normal incident Gaussian beam, the electric field of the coherent Gaussian beam with an incident angle of θ can be approximately expressed as

$$E(x,\theta)=G_0\exp\left[-\left(\frac{x-z_0\sin\theta}{w_0}\right)^2\right]\cdot\exp[-\mathrm{i}k(x-z_0\sin\theta)\sin\theta] \quad (2)$$

where w_0 is the beam waist width, G_0 is a constant . The first factor is due to the shift of the waist center, and the second is due to a θ angle decline of the waist plane . With the help of Collin's formula and the detail information of the two paths, $h_1(x_1, u_1)$and $h_2(x_2, u_2)$ [15], we obtain

$$\langle I(u_1)\rangle=\left|\left(-\frac{1}{\lambda^2 z_3 b_1}\right)^{1/2}\int_{-\infty}^{\infty}\int_{-\infty}^{\infty}E(x_1,\theta)H(v_1)\cdot\exp\left[-\frac{\mathrm{i}\pi}{\lambda b_1}(a_1x_1^2-2x_1v_1+d_1v_1^2)\right]\cdot\exp\left[-\frac{\mathrm{i}\pi}{\lambda z_3}(v_1^2-2v_1u_1+u_1^2)\right]\mathrm{d}x_1\mathrm{d}v_1\right|^2 \quad (3)$$

$$\langle I(u_2)\rangle=\left|\left(-\frac{\mathrm{i}}{\lambda b_2}\right)^{1/2}\int_{-\infty}^{\infty}E(x_1\cdot\theta)\cdot\exp\left[-\frac{\mathrm{i}\pi}{\lambda b_2}(a_2x_1^2-2x_1u_2+d_2u_2^2)\right]\mathrm{d}x_1\right|^2 \quad (4)$$

where a_1,b_1,c_1 and d_1 are the optical transfer matrix elements between the source plane and object, and a_2, b_2, c_2 and d_2 are the optical transfer matrix elements between the source plane and D_2.

$$\begin{pmatrix}a_i & b_i\\ c_i & d_1\end{pmatrix}=\begin{pmatrix}1 & z_i\\ 0 & 1\end{pmatrix}\begin{pmatrix}1 & 0\\ -1/f & 1\end{pmatrix}\begin{pmatrix}1 & z\\ 0 & 1\end{pmatrix}=\begin{pmatrix}1-\frac{z_i}{f} & z+z_i-\frac{z_iz}{f}\\ -\frac{1}{f} & 1-\frac{z}{f}\end{pmatrix},\quad i=1,2 \quad (5)$$

In order to obtain the image(near field image [4]), we need $\frac{1}{z}+\frac{1}{z_1}=\frac{1}{f}$ and $z_1=z_2$ (focusing in both paths), and the second order correlation function becomes

$$G^{(2)}(u_2,\theta)=\langle I(u_2)\rangle\int_{-\infty}^{\infty}\langle I(u_1)\rangle\mathrm{d}u_1=\frac{1}{a_1a_2}\int_{-\infty}^{\infty}\left|H(v_1)\exp\left[-\left(\frac{\frac{v_1}{a_1}-z_0\sin\theta}{w_0}\right)^2\right]\right|^2\mathrm{d}v_1\cdot\exp\left[-2\left(\frac{\frac{u_2}{a_2}-z_0\sin\theta}{w_0}\right)^2\right] \quad (6)$$

where the θ dependence is explicitly expressed. For small beam waist width(w_0=0), we approximately have $(a_{1,2}\neq 0)$

$$G^{(2)}(u_2,\theta)\propto\frac{a_1}{\lambda z_3 a_2}\left|H(z_0a_1\sin\theta)\right|^2\delta\left(\frac{u_2}{a_2}-z_0\sin\theta\right) \quad (7)$$

Please note that the beam in path one gives $\left|H(z_0a_1\sin\theta)\right|$, while the beam in path two gives $\delta\left(\frac{u_2}{a_2}\right)-z_0\sin\theta$. For the beam with a fixed θ, the coincident counting with D_2 at u_2 corresponds to a point of the object in path one through the delta function . The average over θ yields the whole image of the object in the coincident counting(intensity-intensity correspondence).

In a real situation the waist width w_0 is finite, and the imaging can be found numerally from Eq .(6). In Fig.2, we plot normalized $G^{(2)}(u_2,\theta)$versus θ and u_2 for double slits with a small waist width w_0= 0.01 mm, z =2 f and $z/z_{1,2}$= 1. The transmission function of the object is $H(v)$= 1 for $-\frac{h_2}{2}-\frac{h_1}{2}<v<-\frac{h_2}{2}+\frac{h_1}{2}$ and $\frac{h_2}{2}-\frac{h_1}{2}<v<\frac{h_2}{2}+\frac{h_1}{2}$ and = 0 otherwise, where h_1 is the slit width, and h_2 is the distance of the two slits . The other parameters are λ = 702 nm, h_1 =0.1 mm, h_2 = 0.3 mm, z_0 =50 mm. Integrating Eq.(6) over a small range of $\pm\theta_0(\theta_0=0.02\,\mathrm{rad})$, we can obtain the image of the object . In Fig. 3, we plot the average of the normalized second order correlation function, $G^{(2)}(u_2)=\int_{-\theta_0}^{\theta_0}G_{av}^{(2)}(u_2\theta)\mathrm{d}\theta$, for different beam waist widths with z=2f and $z/z_{1,2}$ =1 . The quality of the image is influenced by the beam waist width . The smaller the beam waist width, the better the quality of the image . For large w_0, the quality of the image can be improved by choosing large $z/z_{1,2}$, which results in small spots at the object and D_2. In the inset of Fig. 3, we plot the images for $z/z_{1,2}$= 100 and $\frac{1}{z}+\frac{1}{z_1}=\frac{1}{f}$ with w_0= 1 mm, where we see that the quality

is the same as that for small width w_0= 0.01 mm. Images with high quality and high visibility can be formed .

For very large beam waist width($w_0=\infty$), we can set $z_1=z_2=f$(equivalent $z=\infty$)for the imaging(far field image[4]). Then the second order correlation function becomes

$$G^{(2)}(u_2,\theta)\propto\frac{\lambda}{z_3 f^2}\left|H(f\sin\theta)\right|^2\delta\left(\sin\theta-\frac{u_2}{f}\right) \qquad (8)$$

The beam in path one gives one point of the object, $\left|H(f\sin\theta)\right|$, while the beam in path two gives $\delta(\sin\theta - u_2/f)$ corresponding to a point at detector 2 hit by the coherent beam. The average over θ yields the whole image in the coincident counting . At the plane right after the object, the same image is formed due to the focusing of the source(each θ gives a point, all θ gives the image). Therefore, we can conclude that the image in the coincidence counting is due to the intensity-intensity correspondence between the two detectors . If the detector one is point-like, the coincidence image could not be formed due to the cutoff of the intensity-intensity correspondence, while in the quantum case the coincidence image formation does not depend on whether detector one is a budget one or a point-like one . The lens in the classical case must be before the beam splitter because the function of the lens is focusing(not imaging) for both paths, while in the quantum case, the lens can be in path one or in path two, because its function is imaging(not focusing).

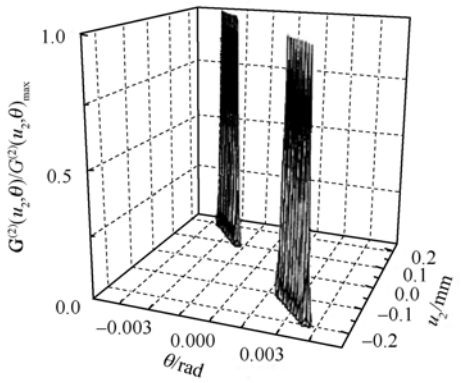

$G^{(2)}(u_2,\theta)$, with w_0=0.01 mm

Fig .2 The second order correlation function

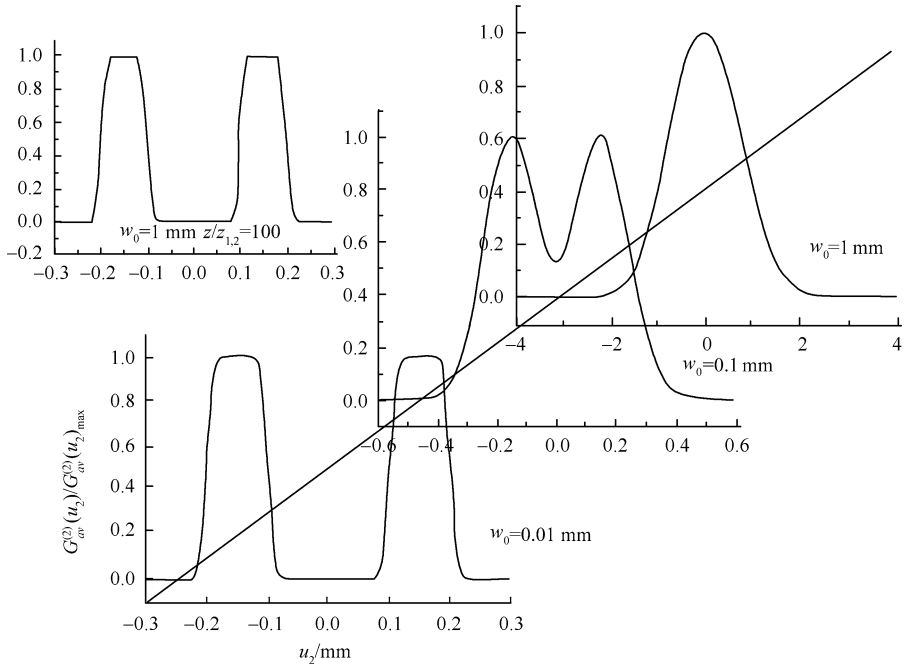

$G^{(2)}_{av}(u_2)$ for different w_0=0.01,0.1 and 1mm at $z/z_{1,2}$=1

Fig .3 The average of the second order correlation function

2 Coincidence interference with coherent Gaussian beams

Now we investigate the coincidence interference with the coherent Gaussian beam, see Fig.4 (the same configuration of Ref.[13]). Here D_1 is a point-like detector fixed at $u_1=0$. The lens is in path two . The coincident counting rate is proportional to $G^{(2)}(u_1=0,u_2)$. With the detail information about the two paths $h_1(x_1, u_2)$and $h_2(x_2, u^2)$, we obtain

$$
\begin{aligned}
&G^{(2)}(u2\cdot\theta)\\
&=\frac{1}{\lambda^3 z_1 z_3 b_2}\exp\left(-\frac{4z_0^2\sin^2\theta}{w_0^2}\right)\left|\sqrt{\frac{\pi}{\frac{1}{w_0^2}+\frac{\mathrm{i}ka_2}{2b_2}}}\right.\\
&\cdot\exp\left[\frac{\left(\frac{(2z_0\sin\theta)}{w_0^2}-\mathrm{i}k\sin\theta_1+\frac{\mathrm{i}k}{b_2}u_2\right)^2}{4\left(\frac{1}{\omega_0^2}+\frac{\mathrm{i}ka_2}{2b_2}\right)}\right]\Bigg|^2\\
&\cdot\left|\int_{-\infty}^{\infty}\sqrt{\frac{\pi}{\frac{1}{w_0^2}+\frac{\mathrm{i}k}{2z_1}}}H(v_1)\right.\\
&\cdot\exp\left[\frac{\left(\frac{\mathrm{i}k}{z_1}v_1+\frac{2z_0\sin\theta}{\omega_0^2}-\mathrm{i}k\sin\theta\right)^2}{4\left(\frac{1}{\omega_0^2}+\frac{\mathrm{i}k}{2z_1}\right)}\right]\\
&\cdot\exp\left(-\frac{\mathrm{i}k}{2z_1}v_1^2-\frac{\mathrm{i}k}{2z_3}v_1^2\right)\mathrm{d}v_1\Bigg|^2
\end{aligned}
\tag{9}
$$

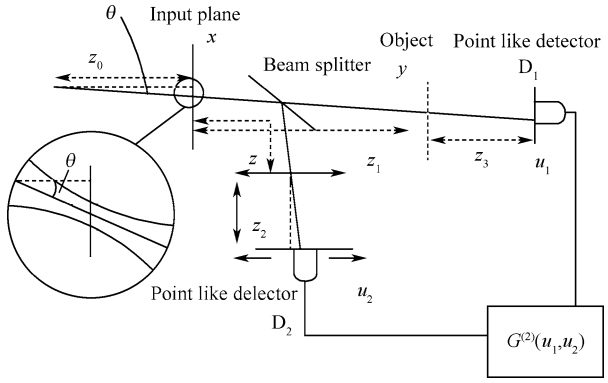

Fig.4 The scheme for coincidence interference with the coherent Gaussian beam

where

$$
\begin{aligned}
\begin{pmatrix} a_2 & b_2 \\ c_2 & d_2 \end{pmatrix} &= \begin{pmatrix} 1 & z_2 \\ 0 & 1 \end{pmatrix}\begin{pmatrix} 1 & 0 \\ -1/f & 1 \end{pmatrix}\begin{pmatrix} 1 & z \\ 0 & 1 \end{pmatrix}\\
&= \begin{pmatrix} 1-\frac{z_2}{f} & z+z_2-\frac{z_2 z}{f} \\ -\frac{1}{f} & 1-\frac{z}{f} \end{pmatrix}
\end{aligned}
\tag{10}
$$

In order to obtain the interference fringes of the double slits, we need to set $z_2=f$ for $w_0=\infty$, and consequently, Eq .(9) approximately reduces to

$$
\begin{aligned}
G^{(2)}(u_2,\theta) &\propto \frac{1}{z_3 f}\sin c^2\left(\frac{h_1\pi\sin\theta}{\lambda}\right)\\
&\cdot\cos^2\left(\frac{h_2\pi\sin\theta}{\lambda}\right)\delta(u_2-f\sin\theta)
\end{aligned}
\tag{11}
$$

The beam in path one gives the interference fringe at the plane of detector one, $\mathrm{sinc}^2(h\pi\sin\theta/\lambda)\cos^2(h_2\ \pi\ \sin\theta/\lambda)$, while the beam in path two gives $\delta(u_2-f\sin\theta)$. For the beam with a fixed θ, the coincident counting with D_2 at u_2 is the correspondence of a point of the interference fringes in path one through the delta function . By varying θ, we can have different points of the interference fringes at different u_2. The average over θ yields the whole interference pattern in the coincident counting. Essentially, the pattern is completely determined by path one, and is the first order interference, which can be easily verified by the equation $\sin\theta=\lambda/2d$ (d is the separation of the two slits)[13]. It is clear that the interference fringes in the coincidence counting are due to the intensity-intensity correspondence between the two detectors plus the first order interference in path one . If the detector one is a budget one, the fringes could not be obtained in the coincident counting, because of the destruction of the correspondence . In the classical case, the lens is necessary for the purpose of focusing . In the quantum case, no lens is needed .

For finite w_0, the interference fringes can be found with numerical calculation from Eq .(9). In Fig 5, we plot the normalized $G^{(2)}(u_2,\ \theta)$ versus θ and u_2 for double slits with finite waist width w_0= 2 mm. In Fig . 6 we plot the average of the normalized second order correlation function, $G_{av}^{(2)}(u_2)$, for different beam waist widths. The parameters used in the calculations are λ=702 nm, h_1= 0.15 mm, h_2= 0.5 mm, z_0=5 mm. θ_0=0.01 rad, f=5 mm, z_1= 5 mm, z_3= 15 cm. From Fig . 6 we see that the fringes disappear when w_0 is small. For small beam waist, the fringes can also be recovered by adjusting the position of the lens to fit the imaging condition, $\frac{1}{z}+\frac{1}{z_2}=\frac{1}{f}$, see the

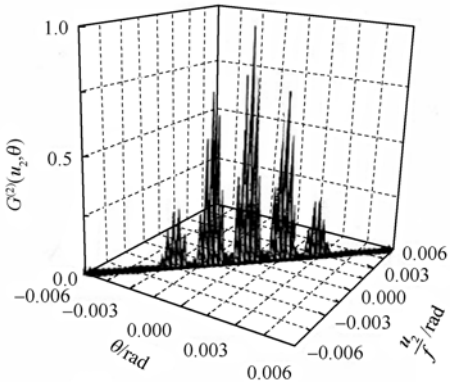

$G^{(2)}(u_2,\theta)$ with w_0= 2 mm and $z_2=f$

Fig .5 The second order correlation function

inset of Fig. 6，where we plot the average of the normalized second order correlation function, $G_{av}^{(2)}(u_2)$ (z =55 mm，and z_2=5.5 mm)for w_0=0.01 mm. Fringes with high quality and high visibility can be obtained in the classical case .

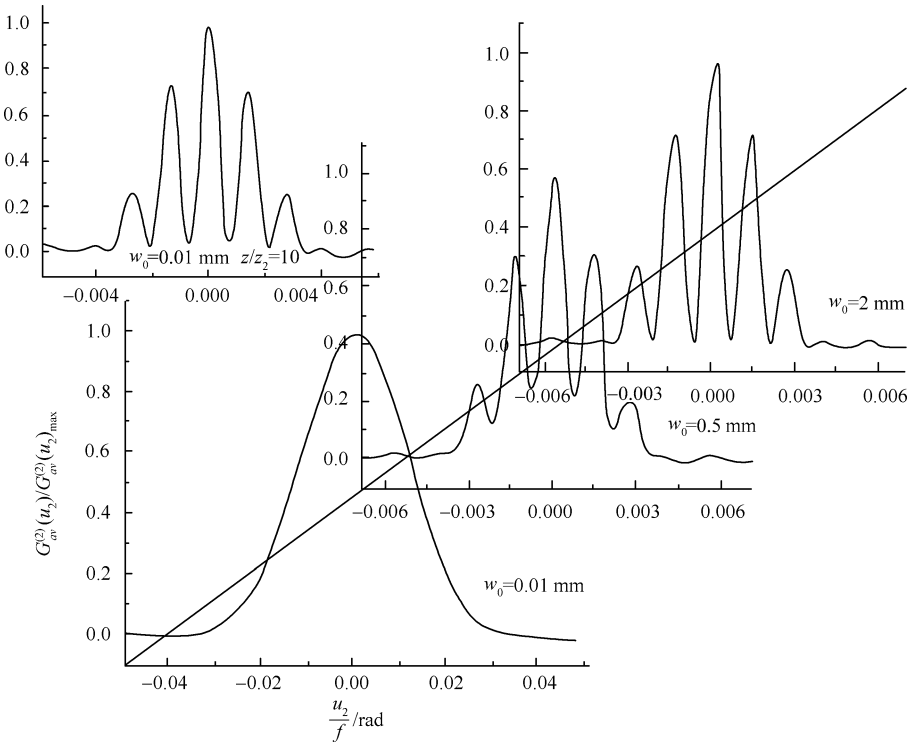

$G_{av}^{(2)}(u_2)$ with $z_2=f$, for different beam waist widths

Fig .6 The average of the second order correlation function

3 Discussion and conclusion

Here we would like to point out that the coincidence imaging with coherent sources is different from that with a random Gaussian source [6–12] whose fluctuations obey Gaussian statistics . A thermal source [14] can be approximately treated as such a source . For such a source we have $G^{(2)}(x_1, x_2)=\langle I(x_1)\rangle\langle I(x_2)\rangle+|\langle E(x_1)E^*(x_2)\rangle|^2$. The second term results in the coincidence images or interference fringes， which is similar to the term $|\langle 0,0|E(x_1)E(x_2)|\Psi\rangle|^2$. in the quantum case . However，there is an additional term，the first one，on which the visibility depends . A perfect image is accompanied by zero visibility[7–8]. High quality and high visibility can t be obtained simultaneously with the random Gaussian source . The nature of the coincidence imaging with the random Gaussian source is the Hanbury Brown-Twiss Effect . Using the same experimental setup in the quantum case [1–2]，the coherent source can not produce the coincidence image or interference fringes，while the random Gaussian source does can produce the coincidence image and interference fringes but with low visibility [7–10]. Besides，the setup with random Gaussian sources can be exactly the same as in the quantum case .

In both the classical coherent and quantum cases，coincidence images and interference fringes with high visibility and high quality can be obtained . However，in the quantum case，the correlation is between their electric field(the probability amplitude correlation)，$G^{(2)}(x_1,x_2)=|\langle 0,0|E(x_1)E(x_2)|\Psi\rangle|^2$，while in the classical coherent case，it is the intensity-intensity correspondence between the two detectors . The images or the interference fringe patterns in the classical coherent case are determined by the path with the object(and the other path provides a correspondence point)，while in the quantum case， the image and interference fringes are determined by both paths due to the wave function correlation (the quantum entanglement). Due to the different physics， the setup with coherent sources is different from the setup in the quantum case . In the classical coherent case，the lens is used for focusing，while in the quantum case, it used for imaging. In conclusion the coincidence imaging and interference with the coherent Gaussian beam are due to the intensity-to-intensity (particle-to-particle) correspondence a classical nature，while those with the entangled photon pairs are due to the coherent superposition of the amplitudes of two electric fields a quantum nature .

Acknowledgments This work was supported by the Research Grants Council of Hong Kong(CA02/03 . SC01)and FRG of Hong Kong Baptist University .

References

1. PITTMAN T. -B.，SHIH Y. -H.，STREKALOV D. V.，et al . Optical imaging by means of two-photon quantum entanglement, Phys Rev A，1995，52：R3429
2. STREKALOV D. -V.，SERGIENKO A. -V.，KLYSHKO D. N.，et al . Observation of two-photon ghost interference and diffraction, Phys Rev Lett，1995，74：3600
3. BENNINK R.-S.，BENTLEY S.-J.，BOYD R.W.，“Two-photon”coincidence imaging with a classical source, Phys Rev Lett，2002，89：113601
4. GATTI A.，BRAMBILLA E.，LUGIATO L. -A., Entangled imaging and wave-particle duality：From the microscopic to the macroscopic realm. Phys Rev Lett，2003，90：133603
5. ANGELO M. -D.，SHIH Y. -H., Can quantum imaging be classically simulated？. quant-ph/0302146
6. GATTI A.，BRAMBILLA E.，BACHE M.，et al . Correlated imaging，quantum and classical, Phys Rev A，2004，70：013802
7. CAI Y.，ZHU S ., Ghost imaging with blackbody radiation, quant-ph/0407240
8. CAI Y.，ZHU S., Ghost interference with partially coherent radiation, Opt Lett，2004，29：2716-2718
9. VALENCIA A.，SCARCELLI G.，ANGELO M. D.，et al . Two-photon “ ghost ” imaging with thermal light. quant-ph/0408001
10. MAGATTI D.，FERRI F.，GATTI A.，et al . Experimental evidence of high-resolution ghost imaging and ghost diffraction with classical thermal light, quant-ph/0408021 .
11. CHEN J.，HAN S ., Incoherent Coincidence Imaging and Its Applicability in X-ray Diffraction, Phys Rev Lett，2004，92：093903
12. WANG K.，CAO D., Sub-wavelength coincidence interference with classical thermal light. Phys Rev A，2004，70：041801
13. BENNINK R. -S.，BENTLEY S. -J.，BOYD R. -W.，et al . Quantum and Classical Coincidence Imaging, Phys Rev Lett，2004，92：033601
14. MANDEL L.，WOLF E., Optical Coherence and Quantum Optics, Cambridge，New York，1995
15. COLLINS S. -A., Lens-system diffraction integral written in terms of matrix optics, J Opt Soc Am，1970，60：1168